





Electrochemical Study of Nickel Electrodeposition from Chloride Solutions onto Glassy Carbon Electrodes

 Luis Humberto Mendoza-Huizar,^{1,*}  Giaan Arturo Álvarez Romero,¹
 Maria Elena Paez Hernández,¹  Margarita Rivera²

¹ Universidad Autónoma del Estado de Hidalgo. Área Académica de Química. Ciudad del Conocimiento, Carretera Pachuca-Tulancingo km. 4.5, CP. 42184 Mineral de la Reforma, Hidalgo, México

² Instituto de Física, Universidad Nacional Autónoma de México, Ciudad de México, 04510, México

* Corresponding author's e-mail address: hhuizar@uaeh.edu.mx

RECEIVED: August 11, 2024 * REVISED: December 11, 2024 * ACCEPTED: December 13, 2024

Abstract: In the present work, we conducted an electrochemical study on nickel electrodeposition on glassy carbon electrode (GCE) from an ammoniacal solution containing 0.01 M NiCl₂ and 0.1 M NH₄Cl. From the voltammetric study, it was possible to calculate the diffusion coefficient's value as $1.93 \times 10^{-6} \text{ cm}^2 \text{ s}^{-1}$. The current density transients were analyzed using a kinetic mechanism model involving three different contributions: (a) a Langmuir-type adsorption process, (b) 3D nucleation limited by a mass transfer reaction, and (c) a proton reduction process. Non-linear fittings of the current density transients revealed that the values of the nucleation rate (*A*) and the number of active nucleation sites (*N₀*) increased with the decrease in the applied overpotential. Morphological studies have confirmed the existence of a progressive nucleation process with Ni crystallites ranging from 0.5 to 4 μm.

Keywords: nickel, electrodeposition, kinetic, proton reduction, glassy carbon.

INTRODUCTION

SINCE the first practical formulation for nickel plating was reported by Bottger in 1843, a significant amount of information about this process has been accumulated.^[1] Traditionally, nickel electroplating has been applied in three main categories: decorative, functional (protective coatings), and electroforming.^[2,3] However, it is well known that nickel particles with controlled growth exhibit properties that can be utilized in novel applications such as electrocatalysis,^[4,5] energy storage,^[6–8] and the construction of fuel cells,^[9] among others. The electrodeposition process of nickel has been extensively studied on stainless steel,^[7,10] iron, and glassy carbon electrodes (GCE),^[5,11–15] among other surfaces.^[16–18] It has been reported that nickel electrodeposition on GCE from ammoniacal solutions follows a progressive nucleation,^[14] while from acid chloride solutions, nickel deposits start their growth as conic,^[19–22] or hemispheric nuclei.^[23] The

use of additives has been a typical method employed to improve the quality of nickel deposits^[24,25] for example, the addition of coumarin or saccharin produces nickel nanoparticles with an average size of 100 nm.^[26]

Other variables analyzed during nickel electrodeposition include pH,^[27,28] temperature,^[28] bath composition,^[29,30] magnetic field influence,^[31] nickel coordination sphere,^[32,33] proton reduction,^[34,35] ultrasound,^[36] current density, and deposition potential.^[37,38] Additionally, it has been reported that the presence of metallic impurities in the plating baths modifies the kinetics of the electrodeposition process and the morphology of nickel deposits.^[30] Several reports in the literature have analyzed the kinetic parameters of the nickel electrodeposition process to predict its nucleation and growth.^[12,13,15,30,39] For example, Torabi et al. studied nickel electrodeposition from sulfate baths containing potassium and sodium tartrate, boric acid, saccharin, and coumarin, and they found that nickel electrodeposition follows an instantaneous

nucleation mechanism with 3D growth.^[35] Grujicic et al. determined that nickel is electrodeposited through a progressive nucleation mechanism from sulfate solutions at different pH values.^[12] Moreover, they detected an inhibition of nickel electrodeposition caused by sulfate adsorption and proton reduction processes.^[12] However, it has been reported that nickel electrodeposits obtained from chloride solutions are brittle and prone to corrosion.^[30] As a result, there is a lack of kinetic studies related to these chloride solutions, despite the well-established understanding that the properties of electrodeposits are influenced by the nucleation and growth processes.^[35] In this context, kinetic studies of nickel deposition on GCE from chloride solutions could provide valuable insights into the nickel deposition process by evaluating the kinetic parameters related to its nucleation and growth process. Therefore, the goal of this study is to perform a detailed kinetic analysis of the electrochemical process of nickel electrodeposition on GCE substrates using a chloride-based aqueous plating solution. Specifically, we aim to evaluate and analyze the kinetic parameters associated with nickel electrodeposition on GCE electrodes, as these parameters are crucial for understanding and optimizing the deposition process.

METHODOLOGY

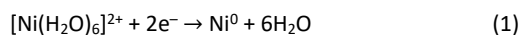
Nickel electrodeposition onto GCE was carried out from an aqueous solution containing 0.01 M of NiCl_2 and 0.1 M NH_4Cl at pH = 7.0 (natural pH). All solutions were prepared using analytical grade reagents with ultra-pure water (Millipore-Q system) and were deoxygenated by bubbling N_2 for 15 minutes before each experiment. All experiments were conducted in a standard three-electrode cell. GCE was a disc-type working electrode with an area of 0.0707 cm^2 , provided by BAS Research Products Company, established in Indianapolis, USA. The GCE electrode was polished with alumina with a particle size of 0.05 microns to achieve a mirror-shiny surface prior to each experiment. A graphite bar electrode with a purity of 99.9995 % of 6.15 mm of diameter and 38.10 mm long, provided by Alfa Aesar Company, was used as the counter electrode. A saturated silver electrode (Ag/AgCl) provided by BAS Research Products Company served as the reference electrode, and all measured potentials are referenced to this scale. In all cases, the experiments were conducted in triplicate to ensure reproducibility. The electrochemical experiments were conducted using an EPSILON potentiostat connected to a personal computer running BASI EPSILON EC software for experiment control and data acquisition. To assess the electrochemical behavior of the electrode in the electrodeposition bath, cyclic voltammetry was performed within the potential range of 0.600 to -1.300 V . In this

voltammetric study, the scan rates used were 10, 20, 30, 40, 50, 60, 70, 80, 90, 100, and 150 mV s^{-1} . A quiet time of 30 seconds was applied in order for the system to reach an equilibrium state, ensuring that the conditions of the electrode are stable before taking a measurement. The kinetic mechanism of nickel deposition onto GCE was investigated under potentiostatic conditions through analysis of the experimental potentiostatic current density transients obtained using the chronoamperometry technique. The potential electrode perturbation always commenced at 0.600 V. The potential step was applied at various potentials as outlined in this study. Also, a quiet time of 30 s was considered in the chronoamperometric study. The characterization of Ni electrodeposits was conducted using a Scanning Electron Microscope (SEM) JEOL JSM6300, manufactured by JEOL Ltd., Japan. This microscope is equipped with a tungsten filament as its electron source and achieves a resolution of 3.5 nm.

RESULTS AND DISCUSSION

Predominance and Pourbaix Diagrams

The chemical composition of a plating bath is crucial in the electrodeposition process. To identify the chemical species of nickel in the deposition bath and their equilibrium potentials, we conducted a thermodynamic study using predominance diagrams. The equilibrium constants for the formation of nickel complexes in aqueous ammoniacal chloride media were obtained from the literature.^[40] The diagrams were plotted using the predominance diagram algorithm implemented in Hydra-Medusa software,^[41] with the results depicted in Figure 1. Figure 1a shows the distribution of nickel chemical species in solution as a function of mole fraction. In the plating bath containing 0.01 M NiCl_2 and 0.1 M NH_4Cl , $[\text{Ni}(\text{H}_2\text{O})_6]^{2+}$ is the predominant species, with a mole fraction of 0.71, followed by NiCl^+ with a mole fraction of 0.21. Therefore, it is clear that at the natural pH of 7, the concentration of $[\text{Ni}(\text{H}_2\text{O})_6]^{2+}$ is maximal. For this reason, we select this specific pH value as the optimal condition for conducting our experiments. Figure 1b presents the Pourbaix diagram of nickel species under the same experimental conditions. According to the Pourbaix diagram at the pH value of 7.0, Ni^{2+} predominantly exists as $[\text{Ni}(\text{H}_2\text{O})_6]^{2+}$ and the equilibrium potential for the $[\text{Ni}(\text{H}_2\text{O})_6]^{2+}/\text{Ni}^0$ couple is -0.497 V vs. Ag/AgCl . Therefore, under these experimental conditions, the nickel reduction process occurs via the following reaction:



Voltamperometric Study

Figure 2 shows the voltammetric data obtained from the GCE/0.01 M NiCl_2 + 0.1 M NH_4Cl system at a scan rate of

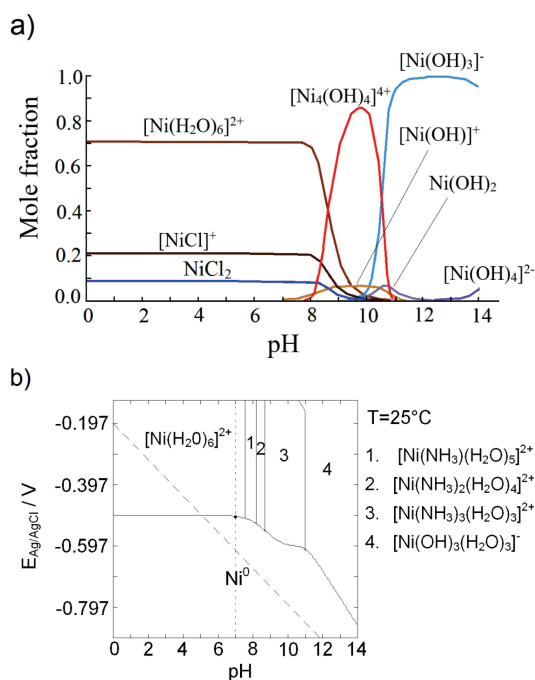


Figure 1. a) Mole fraction predominance diagram showing the distribution of nickel chemical species in solution. b) Pourbaix-type diagrams for the $[\text{Ni}(\text{H}_2\text{O})_6]^{2+}/\text{Ni}^0$ system. In both diagrams, $p\text{Ni(II)} = 2.0$, $p\text{Cl} = 0.0086$, and $p\text{NH}_3 = 1$. The black point in Figure 1b represents our experimental conditions.

20 mV·s⁻¹. During the forward scan, peak A appears at -1.111 V, indicating the onset of the electrocrystallization process at approximately -0.907 V (E_{cris}). After peak A, a significant decrease in current density (j) is observed, corresponding to the proton reduction process.^[42] During the reverse scan, a crossover point at $E_c = -1.071$ V is observed, which is typically associated with an electrocatalytic effect.^[43] A second crossover potential, E_{eq} , was identified at -0.656 V, which is associated with the equilibrium potential of the pair $[\text{Ni}(\text{H}_2\text{O})_6]^{2+}/\text{Ni}^0$. In the anodic region, peak B was recorded at -0.386 V. Peak A is attributed to the direct reduction of $[\text{Ni}(\text{H}_2\text{O})_6]^{2+}$ to Ni^0 , while peak B corresponds to the dissolution of the nickel deposited during the forward scan. It is worth noting that the separation between peaks A and B is 0.725 V, which exceeds 59 mV/n, where n is the number of electrons transferred. This value indicates an irreversible system.^[44] Here, it is important to remember that the Randles-Sevcik equation is capable of predicting the electrochemical behavior of reversible systems involving two soluble chemical species in solution.^[45,46] However, in the present case, the electrochemical system is irreversible and generates an insoluble substance, which can be predicted by the Berzins-Delahay model when the system is diffusion-controlled.^[47]

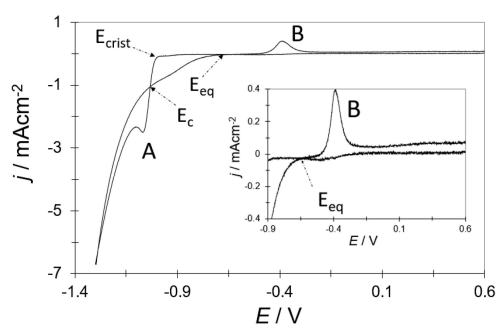


Figure 2. A representative cyclic voltammogram recorded from the GCE/0.01 M NiCl_2 + 0.1 M NH_4Cl system. The potential scan began at 0.600 V in the negative direction with a scan rate of 20 mV s^{-1} .

To determine whether the nickel electrodeposition process is diffusion-controlled, the current density associated with peak A was plotted against $v^{1/2}$ (where v is the scan rate), as shown in Figure 3, using the Berzins-Delahay equation.^[47]

$$j_p = 367n^{3/2}C_0D^{1/2}v^{1/2} \quad (2)$$

In this equation, n is the number of electrons transferred, C_0 is the nickel concentration in moles per liter, D is the diffusion coefficient in $\text{cm}^2 \text{s}^{-1}$, and v is the scan rate in V s^{-1} . The values of current density at the cathodic peak for each scan rate were measured, and a plot of j_p vs. $v^{1/2}$ was generated, where the cathodic peak was identified as the point of maximum current density during the electrochemical reduction. In the present case, a linear relationship between j_p and $v^{1/2}$ was observed, see Figure 3, indicating diffusion control of the nickel electrodeposition process onto the GCE electrode. From the slope of the j_p and $v^{1/2}$ plot, it was possible to evaluate the diffusion coefficient, which was calculated as $1.93 \times 10^{-6} \text{ cm}^2 \text{s}^{-1}$. This value is of the same order of magnitude as the reported value for the electrodeposition of Ni^{2+} in similar systems.^[42,48,49]

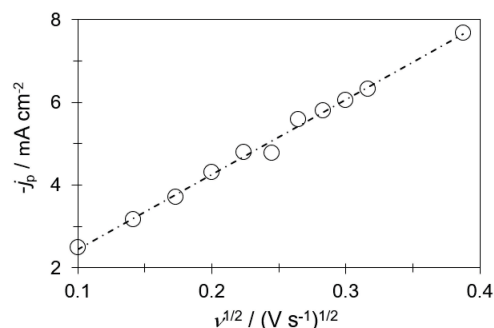


Figure 3. Plot of the experimental cathodic peak current density (j_p) as a function of the square root of the scan rate for peak A according to equation (1). The dashed line represents the linear fit of the experimental data.

Additionally, a plot of the cathodic peak potential (E_p) for peak A versus $\log(v)$ was performed, and it was found that E_p varied linearly with $\log(v)$. The equation obtained is $E_p = -0.1848 \log(v) - 1.4376$. It is important to note that an irreversible process can be described by equation (3):^[50]

$$E_p = -\frac{2.3RT}{(1-\alpha)nF} \log(v) + c \quad (3)$$

where R is the gas constant, T is the absolute temperature (K), F is the Faraday constant, α is the transfer charge coefficient, and c is a constant. Based on equation (3), the value for α_{Ni} during the reduction process is 0.83, which is higher compared to the value obtained for Ni electro-deposition on HOPG electrodes (0.64).^[42]

Chronoamperometric Study

It is widely accepted that chronoamperometric studies and the current-time transients obtained from this technique can be used to analyze the kinetics of the electrodeposition process. By analyzing these current density transients, it is possible to evaluate parameters such as the nucleation rate and the density of active nucleation sites to predict the nucleation and growth processes. Figure 4 depicts a series of current density transients (CDT) recorded at various potentials and during 32 s, using the chronoamperometry technique. It may be observed that at shorter times there is a falling current, which may be associated with the charge of the double layer.^[51] In general, after this initial decrease in the current density, it may be observed the formation of a maximum. However, it is interesting to note that at the transient obtained at -1.040 V, after the initial drop in current, it begins to increase again approximately 7 seconds after the potential is applied, indicating the start of the electrodeposition process. The time between the application of the potential and the onset of the electrocrystallization process is referred to as an induction time. Additionally, note that as the applied potential becomes more negative, this induction time decreases. It is due to that when a potential is applied in an electrochemical system, the ions in the solution begin to move toward the electrode. A more negative potential enhances the availability of ions for nucleation on the surface of the electrode, thereby facilitating the formation of nuclei. This reduces the energy required for the ions to aggregate, accelerating the onset of the nucleation process. By decreasing the activation energy with a more negative potential, nuclei form more rapidly and become more stable and as consequence the induction time is reduced. After this initial induction time the current density passes through a maximum, where this maximum has been related to the nuclei overlapping during a 3D nucleation and growth process.^[52] After this point the CDTs shows a

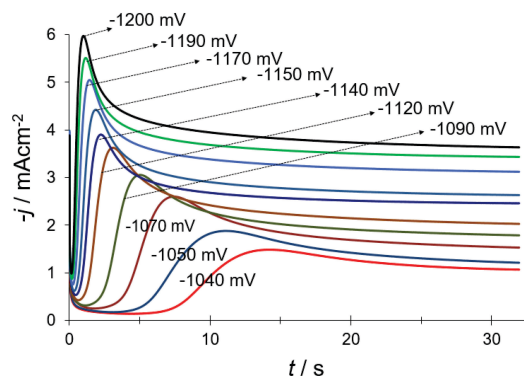


Figure 4. A set of transients recorded from the GCE/0.01 M $NiCl_2$ + 0.1 M NH_4Cl system using the chronoamperometry technique, with various potential step values (mV) as depicted in the figure. In each case, the initial potential was set to 600 mV.

current fall to an approximately constant current density value associated with a planar diffusion of the ions to the electrode surface.^[52]

According to the Cottrell equation, if a system is diffusional controlled then the current density recorded by chronoamperometry exhibit a linear behavior vs. $t^{-1/2}$. For all the transients depicted in Figure 4, we plotted the current density, which decreases after reaching its peak, against $1/t^{1/2}$. However, we did not observe the linear relationship predicted by the Cottrell equation^[53]. Nevertheless, the voltammetric study revealed evidence of diffusion control in the nickel electrodeposition process onto the GCE electrode. Thus, the deviation from the planar diffusion regime may indicate the presence of additional factors influencing the total current during the nickel electrodeposition process via chronoamperometry, aside from the contribution of 3D nucleation. In this context, using the criteria outlined by Sharifker et al., it is possible to classify the nucleation and growth process of nickel based on the CDT shown in Figure 4. Additionally, this type of plot can be used to identify the presence of processes beyond nucleation and growth.^[54] In this procedure, the experimental CDTs are transformed into a non-dimensional form by plotting j^2/j_m^2 against t/t_m , where j_m and t_m correspond to the current density and time values, respectively, at the maximum point recorded in the transient. These experimental data are then compared with the theoretical CDT generated from Eqs. (4) and (5) for instantaneous and progressive nucleation, respectively.^[54]

$$\frac{j^2}{j_m^2} = 1.9542 \left(\frac{t}{t_m} \right)^{-1} \left\{ 1 - \exp \left[-1.2564 \left(\frac{t}{t_m} \right) \right] \right\}^2 \quad (4)$$

$$\frac{j^2}{j_m^2} = 1.2254 \left(\frac{t}{t_m} \right)^{-1} \left\{ 1 - \exp \left[-2.3367 \left(\frac{t}{t_m} \right)^2 \right] \right\}^2 \quad (5)$$

Figure 5 presents a comparison between the theoretical dimensionless transients, derived from equations (4) and (5), and the experimental dimensionless current transients obtained from the GCE/0.01 M NiCl₂, 0.1 M NH₄Cl solution. Notably, for $t/t_m < 1$, the experimental curve closely matches the response predicted for 3D progressive nucleation. However, for $t/t_m > 2.5$, there is a significant deviation from the prediction given by equations (4) and (5). This deviation has been associated with a proton reduction process in the case of metal electrodeposition.^[55]

Palomar-Pardavé et al. have suggested that in systems where proton reduction occurs simultaneously with the diffusion-limited 3D growth of metallic nuclei, the overall current density is described by:^[56]

$$j_{3D}(t) = j_{PR}(t) + j_{3D-dc}(t), \quad (6)$$

where $j_{PR}(t)$ corresponds to the current density contribution from the proton reduction, as given by the equation (7):

$$j_{PR}(t) = \left\{ P_1^* \times \left[1 - \exp \left[(t - t_0) - \frac{1 - \exp(-P_3(t - t_0))}{P_3} \right] \right] \right\} \quad (7)$$

while the current density associated with the nucleation and growth process is described by equation (8)

$$j_{3D-dc}(t) = \left\{ P_4 (t - t_0)^{-1/2} \times \left[1 - \exp \left[(t - t_0) - \frac{1 - \exp(-P_3(t - t_0))}{P_3} \right] \right] \right\} \quad (8)$$

The parameters defined in equations (7) and (8) are provided in equations (9)–(14)

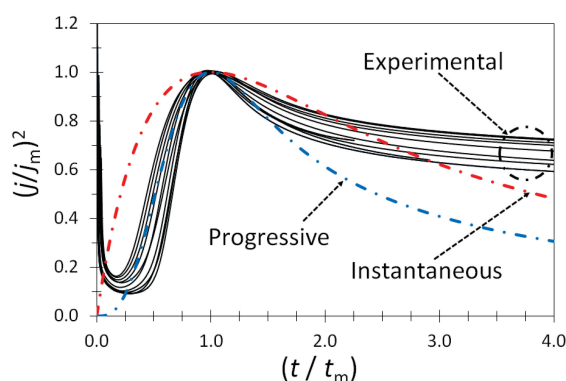


Figure 5. Comparison between an experimental transient normalized by its respective local maximum coordinates (t_m , j_m), and the theoretical dimensionless curves for 3D instantaneous nucleation (Eq. (4)) and 3D progressive nucleation (Eq. (5)).

$$P_1^* = P_1 \left(\frac{2cM}{\pi\rho} \right)^{1/2}, \quad (9)$$

$$P_1 = z_{PR} F k_{PR}, \quad (10)$$

$$P_2 = N_0 \pi k D, \quad (11)$$

$$P_3 = A, \quad (12)$$

$$P_4 = \frac{2FD^{1/2}c}{\pi^{1/2}}, \quad (13)$$

$$k = \left(\frac{8\pi c}{\rho} \right)^{1/2}, \quad (14)$$

where $z_{PR}F$ is the molar charge transferred during the proton reduction process, k_{PR} is the rate constant of the proton reduction reaction, N_0 is the number of active nucleation sites, A is the nucleation rate, F is the Faraday's constant, t_0 is the induction time, and all other parameters have their electrochemical conventional meanings. If the current density is expressed in mA cm⁻², the units of the parameters P_1 , P_2 , P_3 , P_4 , k_1 , k_2 , and t_0 in equations (7)–(14) are as follows: P_1 and P_4 have units of mA cm⁻², P_2 and P_3 are in s⁻¹, k_1 is in mA cm⁻², k_2 is in s⁻¹, and t_0 is in seconds. Also, if we take into account the contribution of the double layer to the initial recorded current, the total current density contribution to the transient may be calculated as follows:

$$j_T = j_{dl} + j_{3D} \quad (15)$$

where

$$j_{dl}(t) = k_1 e^{-k_2 t} \quad (16)$$

$j_{dl}(t)$ is the current density for a Langmuir type adsorption process with $k_1 = k_2 Q_{ads}$ and Q_{ads} is the charge density due to the adsorption process.^[51] By fitting the experimental transients to equation (15), it is possible to obtain the kinetic parameters related to the nucleation and growth process. A nonlinear fit of the experimental transients shown in Figure 4 to equation (15) was performed using the Solver tool in Excel™ with the GRG Nonlinear method.^[57] Random initial values were provided to initiate the optimization process, aimed at minimizing the chi-squared (χ^2) statistic. It is important to note that nonlinear fitting may provide multiple solutions, some of which may not have physical meaning. To avoid this issue, it is advisable to use initial values close to those reported in the literature for similar systems. We allowed the parameters to vary freely within the range of values found in the literature and validated the results by comparing them with those reported in the literature and those obtained from the voltammetric study.

Figure 6 shows a typical comparison between the experimental current transients and those theoretically generated by nonlinear fitting of the experimental data to Eq. (15). It is clear that the model described by this equation accurately describes the total behavior of experimental transients. The physical parameters obtained from the adjustments to Eq. (15) are summarized in Table 1. These values were derived from the parameters P_1 , P_2 , P_3 , and P_4 , which were determined through nonlinear fitting. The average diffusion coefficient from the chronoamperometric study is $2.7 \times 10^{-6} \text{ cm}^2 \text{ s}^{-1}$. A comparison of the diffusion coefficient values from the voltammetric and potentiostatic studies reveals that they fall within the same order of magnitude and are consistent with those reported in the literature.^[48,49] The values of A and N_0 determined in this work are higher and lower, respectively, than those

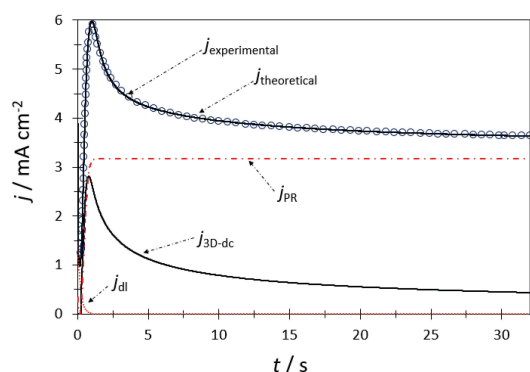


Figure 6. Comparison between the experimental current density transient (—) recorded at -1.200 V and the various theoretical contributions (oooo) generated by nonlinear fitting of Eq. (15). The fit parameters for the adjustment observed in this figure are $P_1 = 3.263 \text{ mA cm}^{-2}$, $P_2 = 8.362 \text{ s}^{-1}$, $P_3 = 1.865 \text{ s}^{-1}$, $P_4 = 1.802 \text{ mA cm}^{-2} \text{ s}^{1/2}$, $k_1 = 1.765 \text{ mA cm}^{-2}$, $k_2 = 1.171 \text{ s}^{-1}$, $t_0 = 0.230 \text{ s}$.

reported for nickel electrodeposition from ammoniacal sulfate solutions at $\text{pH} = 6$ on GCE.^[12] However, it is important to note that the presence of chloride ions in electroplating baths has been shown to accelerate the nucleation process,^[58,59] which was observed in the present study when compared to baths based on sulfates.^[12] The values of N_0 for Ni electrodeposited on different substrates typically fall within the range of $10^6 - 10^7 \text{ cm}^{-2}$,^[35,60] which is consistent with those obtained in the present study. On the other hand, the values for k_{PR} lie within the range reported in the literature, between 10^{-5} and 10^{-9} .^[12,61] Also note that an increase in the values of k_{PR} , A , and N_0 is observed as the applied potential decreases. This may be attributed to a higher concentration of electrons on the electrode surface at lower potentials, which promotes the formation of more nucleation sites and increases the nucleation rate. Additionally, the increased number of Ni nuclei onto the GCE surface enhances proton reduction, thereby increasing k_{PR} . It is also noteworthy that the charge of the double layer remains relatively constant, while the induction time decreases as the applied potential is reduced.

Using the physical constants listed in Table 1, we were able to calculate the saturation nuclear number (N_s) as shown in Table 2. This calculation was performed using Equation (17):^[62]

$$N_s = \left(\frac{AN_0}{2k'D} \right)^{1/2} \quad (17)$$

where

$$k' = \frac{4}{3} \left(\frac{8\pi C_o M}{\rho} \right)^{1/2} \quad (18)$$

From the data reported in Table 2, it can be observed that the N_s values increase as the applied potential

Table 1. Potential dependence of nucleation parameters during nickel electrodeposition onto a glassy carbon electrode from an aqueous solution containing 0.01 M of NiCl_2 + 0.1 M NH_4Cl at $\text{pH} = 7.0$ (natural pH). These values were derived from the best-fit parameters obtained through the fitting process of the experimental j - t plots using Eq. (15)

E / V	A / s^{-1}	$N_0 \times 10^{-6} / \text{cm}^{-2}$	$k_{PR} \times 10^5 / \text{cm}^2 \text{ s}^{-1}$	$Q_{ads} / \text{mC cm}^{-2}$	t_0 / s
-1.04	0.06	1.60	1.93	0.57	6.57
-1.05	0.09	2.08	3.25	0.30	5.39
-1.07	0.16	3.49	5.24	0.29	4.03
-1.09	0.24	4.38	6.64	0.29	2.53
-1.12	0.40	5.56	8.00	0.28	1.32
-1.14	0.84	5.93	11.03	0.36	0.94
-1.15	1.09	5.61	11.57	0.40	0.69
-1.17	1.25	7.31	14.11	0.38	0.45
-1.19	1.66	7.93	15.70	0.38	0.32
-1.20	1.87	8.22	16.51	0.39	0.23

Table 1. Potential dependence of N_s from aqueous solution containing 0.01 M of NiCl_2 + 0.1 M NH_4Cl calculated from physical constants reported in this work (Table 1) and Eq. (17)

E / V	$N_s \times 10^{-5} / \text{cm}^{-2}$
-1.04	1.21
-1.05	1.69
-1.07	2.90
-1.09	4.02
-1.12	5.79
-1.14	8.67
-1.15	9.61
-1.17	11.76
-1.19	14.12
-1.20	15.23

decreases, and these values fall within the range of experimental N_s values reported in the literature.^[63–65] It's worth mentioning that, due to the exclusion zones created by the hemispherical diffusion gradients of 3D nuclei, the N_s values will always be lower than the corresponding N_0 values at the same applied potential. Additionally, both values increase as the applied potential becomes more negative.

Also, from the nucleation rate values reported (see Table 1), it is possible to calculate the Gibbs free energy of nucleation employing the next equation:^[62,66]

$$A = k_3 \exp\left(-\frac{\Delta G}{K_B T}\right) = k_3 \exp\left(-\frac{k_4}{\eta^2}\right) \quad (19)$$

where ΔG is the Gibbs free energy of nucleation, J/nuclei; K_B is the Boltzmann constant ($1.38066 \times 10^{-23} \text{ J mol}^{-1}$), $k_3 = N_0 \omega_{n_c} \Gamma$ where, ω_{n_c} is the frequency of attachment of single atoms to the critical nucleus and Γ is the non-equilibrium Zeldovich factor and depends exponentially on the overpotential.^[67] On the other hand, $k_4 = -(16\pi\gamma^3 M^2 \phi(\theta) / 3\rho^2 z^2 F^2 kT)$, where γ is the interfacial tension of nucleus with its motherphase, $\phi(\theta)$ is a function of the contact angle θ between the nucleus and the substrate.^[67] Here, η is the overpotential, defined as the difference between the applied potential and the equilibrium potential, which in this work was determined from the voltammetric study to be -0.656 V . To determine the Gibbs free energy of nucleation from experimental transients, a plot of $\ln A$ versus η^{-2} can be constructed using Eq. (20). Then, by calculating the slope k_4 of the resulting linear relationship, ΔG can be determined at each specific overpotential using the following equation:^[67]

$$\left(-\frac{\Delta G}{K_B T}\right) = \frac{k_4}{\eta^2} \quad (20)$$

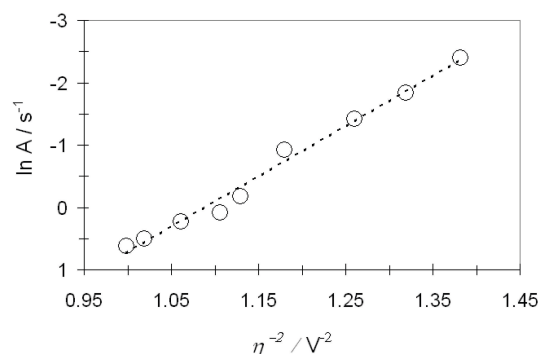


Figure 7. Plot of $\ln A$ versus η^{-2} used to compute the Gibbs free energy of nucleation, as described in Eq. (20). The dashed line represents the linear fit to the experimental data.

where T is the absolute temperature in K, the plot of $\ln A$ vs. η^{-2} (see Figure 7) shows a linear relationship with a slope of -8.1 . The average ΔG calculated at different potentials was $3.87 \times 10^{-20} \text{ J}$ per nucleus. This value of ΔG corresponds to the energy required for the formation of a stable nickel nucleus.

Within the context of the atomistic theory of electrolytic nucleation, the critical size of the Ni nucleus (n_c) can be estimated from the potential dependence of A using the following equation:^[67]

$$n_c = \left(\frac{k_B T}{ze_0}\right) \left(\frac{d \ln A}{dE}\right) - \alpha_{Ni} \quad (21)$$

The plot of $\ln A$ versus E , shown in Figure 8, exhibits a linear trend. By substituting the value of the slope ($d \ln A / dE = -21.5$) into Eq. (21) and $\alpha_{Ni} = 0.83$, the calculated value of n_c is 0. This suggests that each active site on the GCE surface behaves as a critical nucleus.^[43] Similar results have been reported for nickel electrodeposition onto HOPG electrodes.^[42]

$$k_{PR} = k_{PR}^0 \exp\left[-\frac{\alpha_{PR} z F E}{RT}\right] \quad (22)$$

From the slope of the $\ln k_{PR}$ versus E plot shown in Figure 9, the value of α_{PR} was estimated to be 0.13. This value is in close agreement with the 0.07 obtained during the nickel electrodeposition onto Highly Oriented Pyrolytic Graphite (HOPG).^[42] It is important to mention that the reduction of protons (HER) in an electrodeposition process can decrease its efficiency by competing for the electrons that should be used for the reduction of metal cations. Thus, the α_{PR} parameter determines how easily the HER occurs in relation to the metal reduction process.

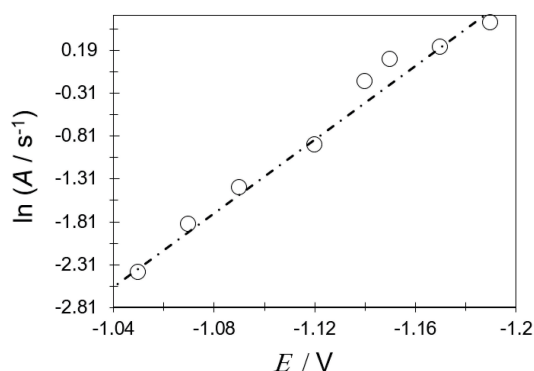


Figure 8. Plot of $\ln A$ versus E , used to calculate the critical size of the Ni nucleus based on Eq. (20). The dashed line represents the linear fit to the experimental data. Additionally, the k_{PR} values reported in Table 1 can be modeled using a Butler–Volmer type relationship,^[56] as described by Eq. (22).

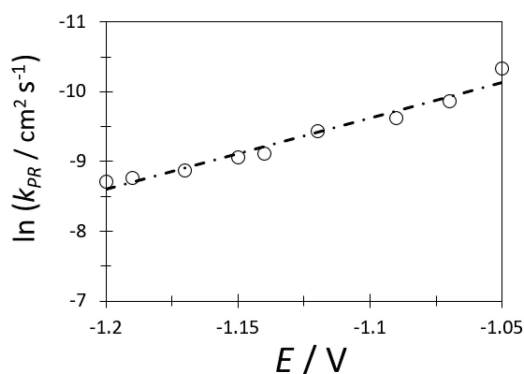


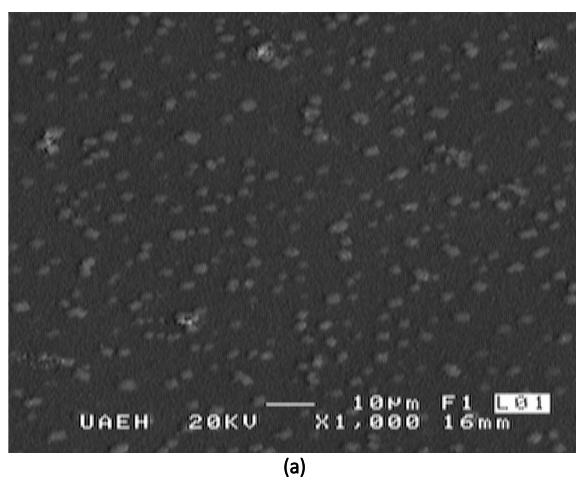
Figure 9. $\ln k_{PR}$ vs. E plot according to Eq. (22). The dashed line corresponds to the linear fit.

Morphological Analysis

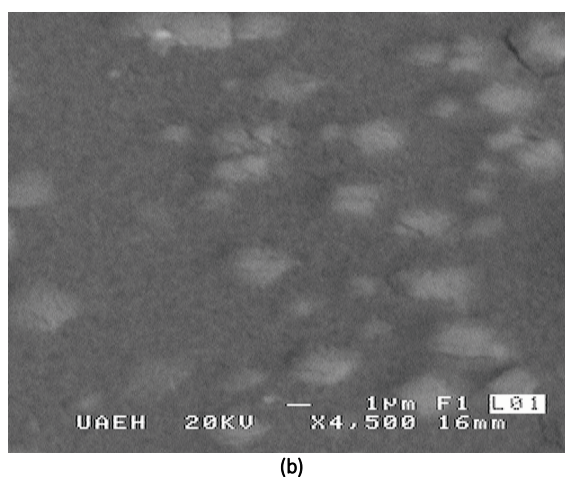
Scanning Electron Microscopy (SEM) was used to examine the morphology of the nickel electrodeposits. The SEM images in Figures 10a and 10b show the electrodeposits formed potentiostatically at -1.090 V, revealing a range of nucleus sizes that reflect the progressive nucleation process observed in the potentiostatic study. Note, the nickel crystallites formed vary in size from 0.5 to $4\ \mu\text{m}$, illustrating the heterogeneous nature of the deposit. Similar morphological features of nickel nuclei have been observed in electroplating steel with nickel from a Watts bath, particularly when saccharin is added.^[68] These results underscore the complex nature of the nickel electrodeposition process, highlighting the importance of evaluating kinetic parameters to optimize and control the properties of electrodeposited materials.

CONCLUSIONS

We investigated the electrodeposition of nickel onto GCE from a $0.01\ \text{M}$ NiCl_2 and $1\ \text{M}$ NH_4Cl aqueous solution using both voltammetric and potentiostatic methods. Our analysis revealed that nucleation parameters, including nucleation rate, density of active nucleation sites, and saturation nucleus, varied with applied potential. The calculated energy (ΔG) required for stable nucleus formation was determined to be $3.87 \times 10^{-20}\ \text{J}$ per nucleus. Additionally, SEM imaging showcased the formation of dispersed particles ranging in size from approximately 0.5 to $4\ \mu\text{m}$. Furthermore, the linear relationship observed in the $\ln k_{PR}$ versus E plot allowed us to estimate α_{PR} as 0.13 , providing further insights into the nucleation process.



(a)



(b)

Figure 10. SEM images of the deposits obtained at $-1090\ \text{mV}$ on GCE from an aqueous solution of $0.01\ \text{M}$ $\text{NiCl}_2 + 0.1\ \text{M}$ NH_4Cl : (a) at $1000\times$ and (b) at $4500\times$ magnification.

Acknowledgments. The authors would like to thank the computer resources, technical expertise and support provided by the Laboratorio Nacional de Supercómputo del Sureste de México, Consejo Nacional de Ciencia y Tecnología (CONACYT) member of the network of national laboratories through the project No. 202203072N and to the Universidad Autónoma del Estado de Hidalgo.

REFERENCES

- [1] G. A. Di Bari, in *Mod. Electroplat. Fifth Ed.* (Eds: M. Schlesinger, M. Paunovic), John Wiley & Sons, Ltd **2011**.
- [2] S. Francis, *Nickel Plating Handbook – Knowledge for a Brighter Future*, 2nd ed., Nickel Institute, Toronto **2023**.
- [3] B. Pierozynski, *Croat. Chem. Acta*. **2012**, 85 (1), 1–8. <https://doi.org/10.5562/cca1743>
- [4] L. Huo, C. Jin, K. Jiang, Q. Bao, Z. Hu, J. Chu, *Adv. Energy Sustain. Res.* **2022**, 3 (4), 2100189. <https://doi.org/10.1002/AESR.202100189>
- [5] K. Pinwattana, R. Janmanee, *NU. Int. J. Sci.* **2015**, 12 (2), 29–38.
- [6] Z. U. Rehman, M. Nawaz, H. Ullah, I. Uddin, S. Shad, E. Eldin, R. A. Alshgari, A. A. A. Bahajjaj, W. U. Arifeen, M. S. Javed, *Mater. 2023, Vol. 16, Page 325*. **2022**, 16 (1), 325. <https://doi.org/10.3390/MA16010325>
- [7] N. Ozdemir, A. Yavuz, P. Y. Erdogan, H. Zengin, *Çanakkale Onsekiz Mart Univ. J. Grad. Sch. Nat. Appl. Sci.* **2019**, 5, 201–213. <https://doi.org/10.28979/comufbed.592527>
- [8] Z. Grubač, A. Sesar, *Croat. Chem. Acta*. **2017**, 90 (2), 273–280. <https://doi.org/10.5562/cca3174>
- [9] Y. M. T. A. Putri, M. I. Syauqi, I. Rahmawati, A. Aliyah, A. R. Sanjaya, T. A. Ivandini, *ChemElectroChem*. **2024**, 11 (5), e202300637. <https://doi.org/10.1002/CELC.202300637>
- [10] Y. Wang, N. Williamson, R. Dawson, N. Bimbo, *J. Appl. Electrochem.* **2023**, 53 (5), 877–892. <https://doi.org/10.1007/S10800-022-01817-4/FIGURES/8>
- [11] B. Meenatchi, V. Renuga, A. Manikandan, *J. Inorg. Organomet. Polym. Mater.* **2016**, 26 (2), 423–430. <https://doi.org/10.1007/S10904-016-0329-3/METRICS>
- [12] D. Grujicic, B. Pesic, *Electrochim. Acta*. **2006**, 51 (13), 2678–2690. <https://doi.org/10.1016/J.ELECTACTA.2005.08.017>
- [13] A. G. Muñoz, D. R. Salinas, J. B. Bessone, *Thin Solid Films*. **2003**, 429 (1–2), 119–128. [https://doi.org/10.1016/S0040-6090\(03\)00277-3](https://doi.org/10.1016/S0040-6090(03)00277-3)
- [14] Y. Xu, Z. Zhu, L. Liu, Z. Liu, *Int. J. Mater. Res.* **2021**, 112 (2), 143–149. <https://doi.org/10.1515/IJMR-2020-8046/MACHINEREADABLECITATION/RIS>
- [15] F. I. Danilov, D. A. Bogdanov, V. S. Protsenko, *Vopr. Khimii i Khimicheskoi Tekhnologii*. **2022**, (2), 3–8. <https://doi.org/10.32434/0321-4095-2022-141-2-3-8>
- [16] G. T. Martínez, G. Zavala, M. Videá, *J. Mex. Chem. Soc.* **2009**, 53 (1), 7–11.
- [17] H. Chiriac, *Thin Solid Films*. **1971**, 8 (5), 345–352. [https://doi.org/10.1016/0040-6090\(71\)90082-4](https://doi.org/10.1016/0040-6090(71)90082-4)
- [18] E. Gómez, R. Pollina, E. Vallés, *J. Electroanal. Chem.* **1995**, 386 (1–2), 45–56. [https://doi.org/10.1016/0022-0728\(95\)03817-Z](https://doi.org/10.1016/0022-0728(95)03817-Z)
- [19] M. Y. Abyaneh, *Electrochim. Acta*. **1991**, 36 (3–4), 727–732. [https://doi.org/10.1016/0013-4686\(91\)85163-2](https://doi.org/10.1016/0013-4686(91)85163-2)
- [20] A. Saraby-Reintjes, M. Fleischmann, *Electrochim. Acta*. **1984**, 29 (4), 557–566. [https://doi.org/10.1016/0013-4686\(84\)87109-1](https://doi.org/10.1016/0013-4686(84)87109-1)
- [21] M. Y. Abyaneh, M. Fleischmann, *Electrochim. Acta*. **1982**, 27 (10), 1513–1518. [https://doi.org/10.1016/0013-4686\(82\)80047-9](https://doi.org/10.1016/0013-4686(82)80047-9)
- [22] M. Y. Abyaneh, W. Visscher, E. Barendrecht, *Electrochim. Acta*. **1983**, 28 (3), 285–291. [https://doi.org/10.1016/0013-4686\(83\)85124-X](https://doi.org/10.1016/0013-4686(83)85124-X)
- [23] J. Amblard, M. Froment, G. Maurin, D. Mercier, E. Trevisan-Pikacz, *J. Electroanal. Chem.* **1982**, 134 (2), 345–352. [https://doi.org/10.1016/0022-0728\(82\)80012-0](https://doi.org/10.1016/0022-0728(82)80012-0)
- [24] Y. L. Zhu, Y. Katayama, T. Miura, *Electrochim. Acta*. **2010**, 55 (28), 9019–9023. <https://doi.org/10.1016/J.ELECTACTA.2010.07.097>
- [25] K. M. Yin, B. T. Lin, *Surf. Coatings Technol.* **1996**, 78 (1–3), 205–210. [https://doi.org/10.1016/0257-8972\(94\)02410-3](https://doi.org/10.1016/0257-8972(94)02410-3)
- [26] Y. L. Zhu, Y. Katayama, T. Miura, *Electrochim. Acta*. **2014**, 123, 303–308. <https://doi.org/10.1016/J.ELECTACTA.2013.12.181>
- [27] M. Boubatra, A. Azizi, G. Schmerber, A. Dinia, *Ionics (Kiel)*. **2012**, 18 (4), 425–432. <https://doi.org/10.1007/S11581-011-0642-3/METRICS>
- [28] G. Q. Zheng, H. Z. Cao, L. F. Zheng, *J. Appl. Electrochem.* **2007**, 37 (7), 799–803. <https://doi.org/10.1007/S10800-007-9313-5/METRICS>
- [29] I. Birlik, N. Funda, A. K. Azem, *J. Sci. Eng.* **2018**, 20 (59). <https://doi.org/10.21205/deufmd.2018205954>
- [30] U. S. Mohanty, B. C. Tripathy, P. Singh, A. Keshavarz, S. Iglaier, *J. Appl. Electrochem.* **2019**, 49 (9), 847–870. <https://doi.org/10.1007/S10800-019-01335-W/METRICS>
- [31] K. Kołodziejczyk, E. Miękoś, M. Zieliński, M. Jaksender, D. Szczukocki, K. Czarny, B. Krawczyk, *J. Solid State Electrochem.* **2018**, 22, 1629–1647. <https://doi.org/10.1007/s10008-017-3875-x>
- [32] Y. Song, J. Tang, J. Hu, S. Liu, Y. Fu, X. Ji, *Electrochim. Acta*. **2016**, 210, 812–820. <https://doi.org/10.1016/J.ELECTACTA.2016.06.033>

- [33] M. J. Deng, I. W. Sun, P. Y. Chen, J. K. Chang, W. T. Tsai, *Electrochim. Acta*. **2008**, 53 (19), 5812–5818. <https://doi.org/10.1016/J.ELECTACTA.2008.03.040>
- [34] E. Chassaing, M. Jousselein, R. Wiert, *J. Electroanal. Chem. Interfacial Electrochem.* **1983**, 157 (1), 75–88. [https://doi.org/10.1016/S0022-0728\(83\)80377-5](https://doi.org/10.1016/S0022-0728(83)80377-5)
- [35] M. Torabi, A. Dolati, *J. Appl. Electrochem.* **2010**, 40 (11), 1941–1947. <https://doi.org/10.1007/S10800-010-0170-2/METRICS>
- [36] I. Tudela, Y. Zhang, M. Pal, I. Kerr, T. J. Mason, A. J. Cobley, *Surf. Coatings Technol.* **2015**, 264, 49–59. <https://doi.org/10.1016/J.SURFCOAT.2015.01.020>
- [37] A. M. Rashidi, A. Amadeh, *Surf. Coatings Technol.* **2008**, 202 (16), 3772–3776. <https://doi.org/10.1016/J.SURFCOAT.2008.01.018>
- [38] N. P. Wasekar, P. Haridoss, S. K. Seshadri, G. Sundararajan, *Surf. Coatings Technol.* **2016**, 291, 130–140. <https://doi.org/10.1016/J.SURFCOAT.2016.02.024>
- [39] J. Aldana-González, M. Romero-Romo, J. Robles-Peralta, P. Morales-Gil, E. Palacios-González, M. T. Ramírez-Silva, J. Mostany, M. Palomar-Pardavé, *Electrochim. Acta*. **2018**, 276, 417–423. <https://doi.org/10.1016/J.ELECTACTA.2018.04.192>
- [40] A. Dean, J., *Handbook of Chemistry*, Fifteenth ed., McGraw-Hill, Inc, New York **1999**.
- [41] I. Puigdomenech, HYDRA (Hydrochemical Equilibrium-Constant Database) and MEDUSA (Make Equilibrium Diagrams Using Sophisticated Algorithms) Programs. KTH Royal Institute of Technology: Stockholm **2004**. <https://www.scirp.org/reference/referencespapers?referenceid=612203> (accessed 2024-04-11).
- [42] L. H. Mendoza-Huizar, (In press) Nickel electrodeposition from an aqueous solution of ammonium chloride onto a Highly Oriented Pyrolytic Graphite (HOPG) electrode: A kinetic and morphological study. *Rev. Mex. Ing. Quim.* **2024**, In press, 1–21.
- [43] S. E. Group, in *Instrum. Methods Electrochem.* (Eds: R. Greef, R. Peat, L. M. Peter, D. Pletcher, J. Robinson), 1st ed., Vol. 1, Woodhead Publishing, Chichester **1985**.
- [44] A. J. Bard, L. R. Faulkner, *Electrochemical Methods and Applications*, 2nd ed., John Wiley & Sons, Ltd **2001**.
- [45] J. E. B. Randles, *Trans. Faraday Soc.* **1948**, 44 (0), 327–338. <https://doi.org/10.1039/TF9484400327>
- [46] A. Sevcik, *Collect. Czechoslov. Chem. Commun.* **1948**, 13, 349–377.
- [47] T. Berzins, P. Delahay, *J. Am. Chem. Soc.* **1953**, 75 (3), 555–559. <https://doi.org/10.1021/ja01099a013>
- [48] Y. Zheng, X. Zhou, Y. Luo, P. Yu, *RSC Adv.* **2020**, 10 (28), 16576–16583. <https://doi.org/10.1039/d0ra00351d>
- [49] N. V. Sotskaya, L. V. Sapronova, O. V. Dolgikh, *Prot. Met. Phys. Chem. Surfaces.* **2014**, 50 (1), 22–26. <https://doi.org/10.1134/S2070205114010134>
- [50] E. Laviron, *J. Electroanal. Chem.* **1979**, 101 (1), 19–28. [https://doi.org/10.1016/S0022-0728\(79\)80075-3](https://doi.org/10.1016/S0022-0728(79)80075-3)
- [51] M. H. Hölzle, U. Retter, D. M. Kolb, *J. Electroanal. Chem.* **1994**, 371 (1–2), 101–109. [https://doi.org/10.1016/0022-0728\(93\)03235-H](https://doi.org/10.1016/0022-0728(93)03235-H)
- [52] B. R. Scharifker, J. Mostany, *J. Electroanal. Chem.* **1984**, 177, 13–23.
- [53] F. G. Cottrell, *Zeitschrift für Phys. Chemie.* **1903**, 42U (1), 385–431. <https://doi.org/10.1515/ZPCH-1903-4229>
- [54] B. Scharifker, G. Hills, *Electrochim. Acta.* **1983**, 28 (7), 879–889. [https://doi.org/10.1016/0013-4686\(83\)85163-9](https://doi.org/10.1016/0013-4686(83)85163-9)
- [55] C. H. Rios-Reyes, L. H. Mendoza-Huizar, M. Rivera, *J. Solid State Electrochem.* **2010**, 14 (4). <https://doi.org/10.1007/s10008-009-0816-3>
- [56] M. Palomar-Pardavé, B. R. Scharifker, E. M. Arce, M. Romero-Romo, *Electrochim. Acta.* **2005**, 50 (24), 4736–4745. <https://doi.org/10.1016/j.electacta.2005.03.004>
- [57] L. S. Lasdon, F. R. L., M. W. Ratner, *Van Nostrand's Sci. Encycl.* **1974**, 73–104. <https://doi.org/10.1002/9780471743989.vse9104.pub2>
- [58] G. Gunawardena, D. Pletcher, A. Razaq, *J. Electroanal. Chem. Interfacial Electrochem.* **1984**, 164 (2), 363–367. [https://doi.org/10.1016/S0022-0728\(84\)80218-1](https://doi.org/10.1016/S0022-0728(84)80218-1)
- [59] A. G. Muñoz, S. B. Saidman, J. B. Bessone, *J. Electrochem. Soc.* **1999**, 146 (6), 2123–2130. <https://doi.org/10.1149/1.1391902/XML>
- [60] X. Zhou, Y. Wang, Z. Liang, H. Jin, *Materials (Basel).* **2018**, 11 (7), 1124. <https://doi.org/10.3390/MA11071124>
- [61] M. Rezaei, S. H. Tabaian, D. F. Haghshenas, *Electrochim. Acta.* **2013**, 87, 381–387. <https://doi.org/10.1016/j.electacta.2012.09.092>
- [62] J. Mostany, J. Mozota, B. R. Scharifker, *J. Electroanal. Chem. Interfacial Electrochem.* **1984**, 177 (1–2), 25–37. [https://doi.org/10.1016/0022-0728\(84\)80208-9](https://doi.org/10.1016/0022-0728(84)80208-9)
- [63] W. Liu, T. Z. Yang, Q. H. Zhou, D. C. Zhang, C. M. Lei, *Trans. Nonferrous Met. Soc. China (English Ed.)* **2012**, 22 (4), 949–957. [https://doi.org/10.1016/S1003-6326\(11\)61269-7](https://doi.org/10.1016/S1003-6326(11)61269-7)
- [64] A. S. Bravo-Rodríguez, L. H. Mendoza-Huizar, M. Rivera, G. A. Álvarez-Romero, *C 2024, Vol. 10, Page 55.* **2024**, 10 (2), 55. <https://doi.org/10.3390/C10020055>
- [65] G. Gunawardena, G. Hills, I. Montenegro, B. Scharifker, *J. Electroanal. Chem.* **1982**, 138 (2), 255–271. [https://doi.org/10.1016/0022-0728\(82\)85082-1](https://doi.org/10.1016/0022-0728(82)85082-1)

- [66] A. Serruya, J. Mostany, B. R. Scharifker, *J. Electroanal. Chem.* **1999**, 464 (1), 39–47.
[https://doi.org/10.1016/S0022-0728\(98\)00464-1](https://doi.org/10.1016/S0022-0728(98)00464-1)
- [67] A. Milchev, *Electrocrystallization. Fundamentals of Nucleation and Growth*, 1st ed., Vol. 1, Kluwer Academic Publishers, Dordrecht **2002**.
- [68] R. Riastuti, S. T. Siallagan, A. Rifki, F. Herdino, C. Ramadini, *IOP Conf. Ser. Mater. Sci. Eng.* **2019**, 541 (1).
<https://doi.org/10.1088/1757-899X/541/1/012053>